EFFECT OF OVERHANG ON WIND-DRIVEN RAIN LOAD OF A MID-RISE BUILDING: FIELD MEASUREMENTS

[1]Hua Ge, [2]Vincent Chiu, [1]Ted Stathopoulos, [1]Firouzeh Souri

[1]Dept. of Building, Civil and Environmental Engineering, Concordia University

hua.ge@concordia.ca

ABSTRACT

Wind-driven rain (WDR) can be considered as one of the most important boundary conditions and moisture sources that influences hydrothermal performance and durability of building envelopes. Given that the deposition of rainwater over building façade and its penetration through the cladding may lead to several types of defects and failures, applying roof overhangs can be considered as an effective feature in building envelope design that provides some degree of protection. Previous experimental studies and CFD modelling have shown that roof overhangs shelter the building facade from WDR. However, there is very limited information on the quantitative evaluation of the overhang effectiveness in protecting the building facade from WDR, especially through field measurements under real-life conditions.

A six-storey mid-rise building with a low-sloped roof located in Vancouver has been fully equipped with a retractable overhang along with a rooftop weather station, a horizontal rain gauge and sufficient number of WDR gauges strategically mounted on the building facades. The spatial distribution of WDR on the building façade has been studied without and with overhang under real-life conditions. The effectiveness of overhang was calculated using two methods: similarity and symmetry. Field measurements show that for the particular climate characterized by long rainy winters with mild wind and rain, the overhang is effective and significantly reduces WDR for this six-story building, especially for areas directly underneath the overhang. The protection increases from the side edge to the center and from the bottom to the top of the façade. The protection provided by the overhang can extend to about half building height. As expected, the larger overhang provides a greater protection and an exponential relationship of overhang width and its effectiveness has been observed.

INTRODUCTION

Wind-driven rain (WDR) is rain that falls obliquely since it is given a horizontal velocity component by the wind. It is one of the most important environmental loads and the main moisture source that affects the hygrothermal performance and durability of building envelopes. Excessive moisture accumulation on porous materials may lead to water penetration, freeze-thaw damage, efflorescence, cracking, and facade soiling. Furthermore, water penetration may lead to the chemical breakdown of organic materials (such as

wood), mould growth, and may reduce the effectiveness of insulating materials (Kumaran et al., 2008). In fact, the amount of rainwater that impinges on the vertical surface of building envelopes under the influence of wind, is the result of complex interactions among wind, rain and buildings. The quantity and spatial distribution of WDR is affected by a wide range of parameters including wind speed, wind direction, rainfall intensity, building geometry, location on building facades, and surrounding topography (Blocken et al., 2004). The importance of WDR has led to intensive research efforts in the past. In recent years, the application of advanced numerical modelling (Abuku at al., 2009; Blocken et al. 2006; Derome at al., 2017; Huang et al., 2010; Kubilay et al. 2013, 2014, 2017and Pettersson et al., 2016) and efforts in collecting high quality and high-resolution measurements (Blocken at al., 2005; Den Nath et al., 2015; Kubilay at al., 2014 and Nore et al., 2007) have advanced our understanding of this complex phenomenon such as the effect of building size, configurations and geometrical details, local weather conditions, and turbulence dispersion (Blocken et al. 2002, 2006, 2009, 2010, 2011; Briggen at al., 2009 ; Deb Nath et al., 2015; Etyemezian at al., 2000; Foroshani at al. 2013; Kubilay et al., 2014, 2015, 2017 and Lalehal et al., 1995).

Roof overhangs have been traditionally used for several purposes including protection against rain. Previous studies show that the shapes of roofs and overhangs have a significant impact on the amount of WDR deposited on building façades. Pitched roofs and overhangs protect the walls below them by shadowing and redirecting airflow (Blocken et al. 2006 and Inculet et al. 1995). Field observations have shown that roof overhangs are effective in certain climates. For example, the field survey on building envelope failures in Southern British Columbia showed that walls with wider overhangs had fewer moisture problems. Field measurements of WDR carried out by Ge and Krpan (Ge et al. 2009) in the same region showed that by having typical overhangs (0.3-0.6 m width) on low-rise buildings and a 0.9 m overhang on a 12-story high-rise building, the deposition of WDR on the building can be significantly reduced, especially at the upper portion of the facade. By reducing the amount of WDR impinged on the top of the façade will also reduce the rainwater runoff that will add to moisture load to the lower portion of the façade. A comprehensive analysis of the effect of roof overhang on the WDR wetting of a low-rise cubic building using CFD modeling was carried out by Foroushani et al. (2013). The influence of wind speed, wind angle, and rainfall intensity was investigated for various overhang sizes. All the tested overhangs protected the upper half of the façade from WDR under the wind and rain conditions examined. The lower half of the façade, however, remained almost unaffected by the overhang. The protective effect of the overhang increases with the increase of overhang width and decreases with the increase of wind speed. Compared to rainfall intensity, both wind speed and wind angle have much greater impact on the WDR loads and the performance of overhangs. Most recently, Kubilay et al. (2017) investigated the effect of overhang and balcony projection on the WDR wetting of the façade through CFD modeling.

Although some field observations have shown that overhangs are effective in reducing WDR wetting of building facades under certain climatic conditions, there has not been any systematic study on quantifying the effect of overhangs on WDR loads, especially through field measurements. In many previous studies, overhangs are part of the buildings on which data is collected. The existence of the overhang is, thus, merely reported rather than being studied as a parameter. The design practice has been generally based on rules-of-thumb and governed by the architectural expression. Given the level of skepticism in the construction community on the utility of overhangs on taller buildings, and the under-appreciation of the importance of overhangs in protecting WDR in contemporary design practice, it is important that data be

generated to evaluate and quantify the effect of overhang on WDR acting on mid-rise and high-rise buildings.

The objective of this research is to quantify the effectiveness of roof overhangs in reducing WDR loads on building façades under real life conditions through field measurements. A unique adjustable overhang has been installed on a six-story building in Vancouver and over three-year's WDR data has been collected and analyzed for various sizes of overhangs. This is the first time, to the best of the authors' knowledge, that the effect of overhangs on WDR wetting of façades has been quantified through field measurements. The field data is also required to validate a CFD model, which will be used for a systematic study of various overhang designs under various climatic conditions. Ultimately, these research efforts will lead to recommendations on effective roof overhang designs for various types of buildings and climates.

MEASUREMENT SETUP

Test Building

The building studied is a six-storey rectangular residential building with a flat roof and a short parapet located near the Burnaby/Vancouver border in British Columbia. The building sits atop an escarpment with the east façade facing the direction of the escarpment and is surrounded by 3-storey residential buildings to its north and west and a highway to its east and south (Figure 1). The building is 39.2 m long, 15.2 m wide, and 19.8 m high. The building facades face the cardinal directions with one of the long faces facing the east perpendicular to the prevailing wind direction during rain hours (Morris, 2006 and Zhu, et. al., 1995). It is a fairly open site within a suburban setting making it an ideal building for wind-driven rain studies.

Figure 1: Satellite images of residential building and its surroundings, Vancouver (https://www.google.ca/maps, August 21st, 2016)

Instrumentation

The installed equipment consists of a customized retractable overhang, an anemometer, a temperature and

relative humidity probe, a horizontal rain gauge, and 31 customized driving rain gauges. The retractable overhang was designed as a permanent structure on the rooftop and can withstand the wind and environmental loads as required by the building code. It is made up of an aluminum framing structure controlled by motor for the adjustment to represent different widths of overhang. The retractable overhang can be changed in width ranging from 0 to 1.2 m and located at the northeast corner of the building covering 15 m of the east façade and 10 m of the north façade. It is attached to the parapet wall (photo in Fig. 2)

The wind monitor measures the wind speed and the wind direction. It is mounted on top of a tripod cross-arm that is 4.6 m above the mechanical room that is located on top of the main roof. It can measure wind speed with a range of 0–50 m/s with an accuracy of ±0.2 m/s or 1% of reading and measure wind direction within a range of 0–360° with an accuracy of ±0.3°. The horizontal rain gauge has a conical collection area (24.5 cm diameter) constructed of gold anodized spun aluminum. The resolution of the tipping bucket is 0.1 mm/tip. The driving rain gauges are customized aluminum plate-type gauges consisting of a square collection area, 30.5 cm by 30.5 cm, for a collection area of 930.3 cm2. The rain gauge was designed with details to minimize measurement errors. The choice of aluminum plate was made considering durability and good surface water runoff to reduce the adhered water. The collector's rim height is kept at 25.4 mm - a low profile to minimize wind errors. The WDR gauge has a dual tipping-bucket mechanism with a resolution of 0.06 mm/tip.

Location of WDR Measurements on Facades

Locations of driving rain gauges on building façades were selected strategically based on prevailing wind direction, building geometry and surroundings. Historical data collected from Environment Canada`s National Climate Services were analyzed to identify the prevailing wind direction during rain, which is from the east. Therefore, a greater number of driving rain gauges are installed on the building east façade. To capture the distribution of WDR on façade, the driving rain gauges were placed at various locations both horizontally and vertically with a focus at the top and corners to create a grid representing a typical wetting pattern on façades. These gauges were typically installed vertically along the corner of the façade at varying heights i.e. 0.61m (2'), 2.44m (8'), 4.88m (16') and 9.14m (30') below the top of the parapet. Figure 2 shows the locations of on-site weather station and the exact WDR gauge locations on building facades.

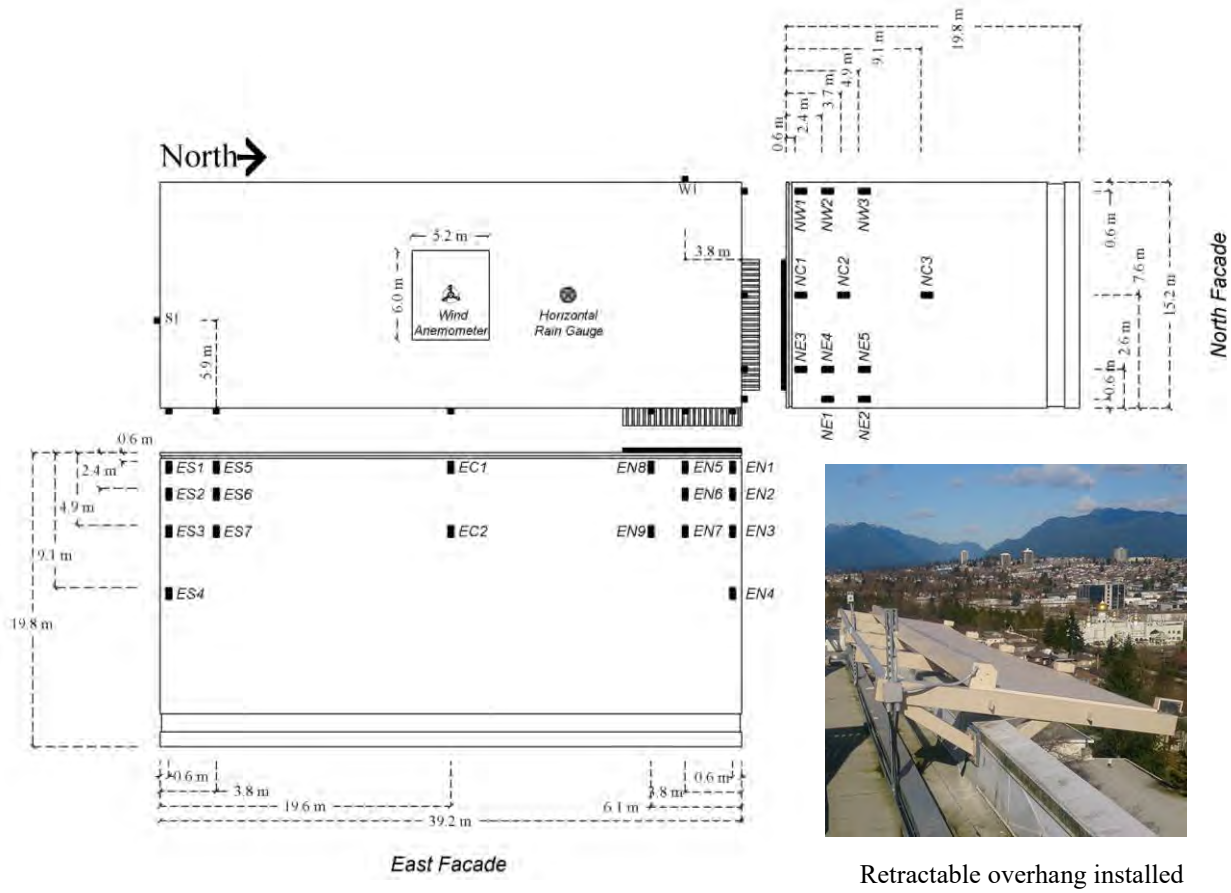

Retractable overhang installed

Figure 2: Location of on-site weather station and WDR gauges on the east and north façades

Data Collection and Processing

All measuring instruments were connected to a central data logger, which was programmed to collect and store raw data every 5 minutes. Wind speed, wind direction, temperature and relative humidity are averaged every 5 minutes. The number of tips is registered also every 5 minutes for the horizontal and the WDR gauges. The data logger is connected to the internet via Ethernet, which allows the data to be collected remotely. Arithmetic-averaging is applied to obtain hourly data that is used in WDR analysis.

The data analysis reported in this paper includes on-site weather conditions, spatial distribution of WDR using catch ratios, and effectiveness of overhang. The on-site wind data have been verified by comparison with data reported by Environment Canada from surrounding weather stations (Chiu, 2016). The spatial distribution of WDR on building facades was analyzed for four cases: no overhang, 0.6 m, 0.9 m and 1.2 m overhang. The effectiveness of each roof overhang in reducing the amount of WDR on façade was assessed.

Data analysis reported in this paper is based on measurements collected from August 2013 to March 2017. This period is divided into four sub-periods:

1) No Overhang: 16 August 2013 to 1 December 2014 (456 days)

2) 4 feet OH (1.2 m): 2 December 2014 to 1 March 2015 and 3 December 2015 to 21 April 2016 (263 days)

3) 2 feet OH (0.6 m): 2 March 2015 to 2 December 2015 (275 days)

4) 3 feet OH (0.9 m): 22 April 2016 to 31 March 2017 (346 days)

RESULTS AND DISCUSSION

On-site Weather Conditions

Figure 3 and Figure 4 show the frequency distribution of wind direction and wind speed measured at the anemometer height during all hours and during rain hours for the four sub-periods, respectively. Rain hours refer to the hours during which horizontal rainfall is registered. Figure 5 shows the frequency analysis of rainfall intensity recorded over the four sub-periods.

Similar wind direction and wind speed frequency distributions are observed over the four monitoring periods. The prevailing wind direction for "all hours" and "rain hours" is from the east, however, the frequency of easterly winds increases significantly during rain hours. Winds are also quite frequent from the east-south-east and east-north-east directions. This narrow band of wind directions coming from the east-north-east to east-south-east, creates an ideal opportunity to study WDR on the east facade, since the prevailing wind is blowing approximately normal to the wall.

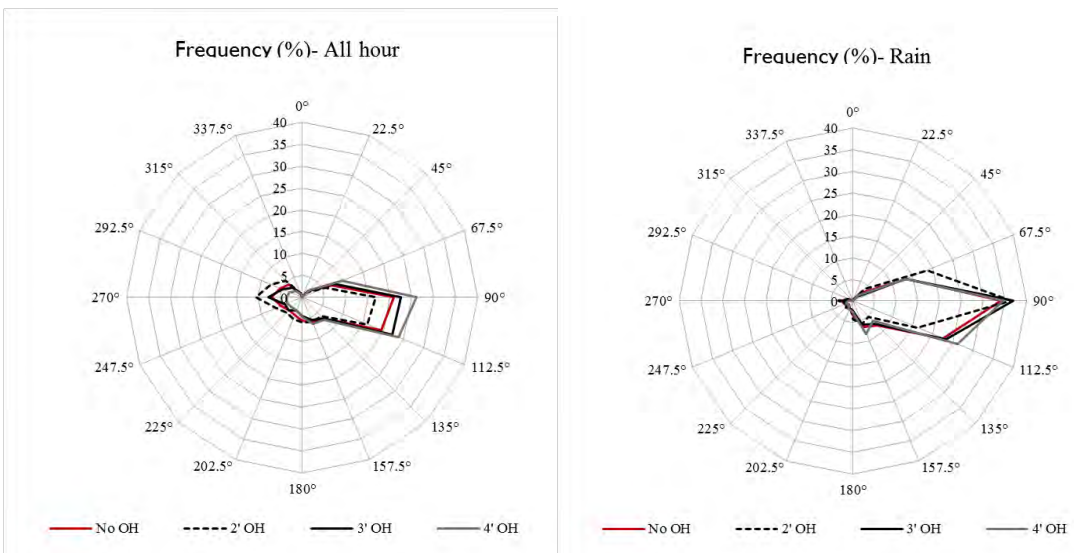

(a) **(b)**

Figure 3: Frequency distribution of wind direction (a) all hours and (b) rain hours for the four sub-periods

Typically, the wind speed is higher during rain hours. Wind speed in the range of 0 to 2 m/s is less frequent during rain hours, which is about 40% of the time, while the majority of wind speed is in the range of 2 to 4 m/s with a frequency of about 50%. Higher wind speeds in the range of 4 to 6 m/s contribute less than 10% of the time and wind speeds greater than 6 m/s have a very low frequency.

During all hours, the frequency is 61% in the range of 0 to 2 m/s, 33% in the range of 2 to 4 m/s and 5% in the range of 4 to 6 m/s, respectively. Rainfall intensity is mostly light to moderate with less than 2 mm/hr for the majority of the time (83%), 2 to 4 mm/hr sometimes (~14%) and rarely over 4 mm/hr.

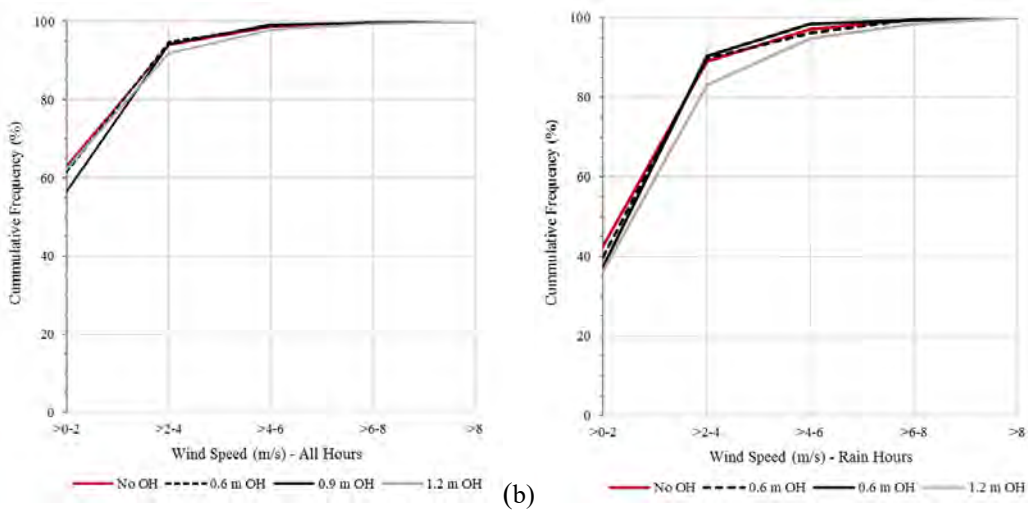

Figure 4: Cumulative frequency of wind speed for all hours (a) and rain hours (b) for sub-periods of study

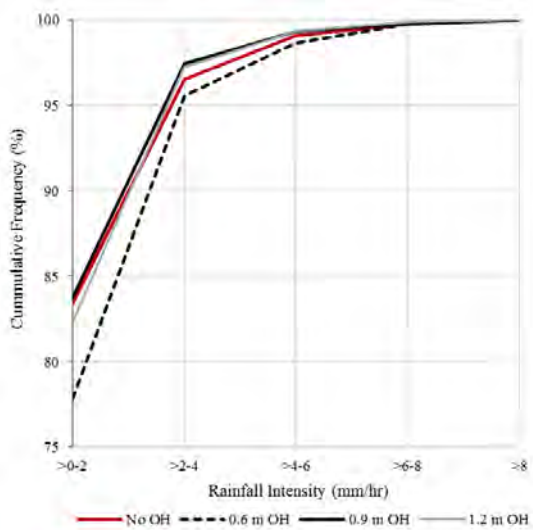

Figure 5: Cumulative frequency of rainfall intensity for sub-periods of study

On-site weather data analysis shows similar wind and rain conditions over the four monitoring periods, which allows the comparison of catch ratios on façade with and without overhang during different monitoring periods to assess the effectiveness of overhangs. This approach is referred to as similarity (repeatability), which will be discussed in the "Similarity" section.

Catch Ratio

Catch ratio provides the basics to understand the spatial distribution of WDR on the building façade and it is defined as the ratio of WDR intensity impinged on the vertical façade of the building (R_{Wdr}) to the horizontal rainfall intensity (equation 1).

$$\eta = \frac{R_{Wdr}}{R_h} \tag{1}$$

Catch ratio is calculated for each monitoring period in order to provide primary understanding of wetting pattern of the façade and how it is influenced by applying overhang with different widths over the roof top of the building and to evaluate the effectiveness of overhang.

Figure 6 shows the catch ratios calculated over the four periods on the east façade. The amount of rain deposited on the building façade, indicated by the catch ratio, varies with location, however, a symmetrical distribution of WDR across the east facade can be observed during the period without overhang (Fig. 6a) given that the prevailing wind direction is from the east most of the time resulting in the wind blowing normal to the façade. The classic wetting pattern can be observed: (1) the top corners are the most wetted followed by the top and side edges and (2) wetting increases from the bottom of the facade to the top and from the middle of the facade to the sides.

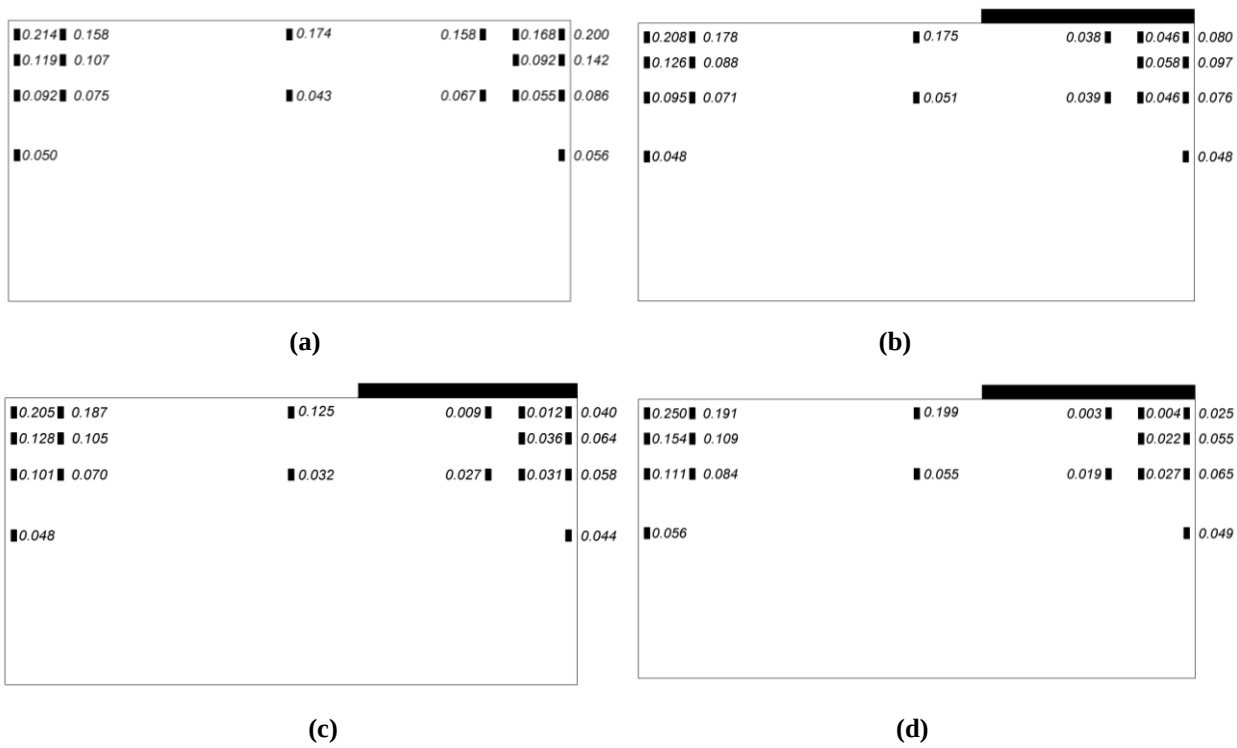

Figure 6: Catch ratios on the east façade: (a) no overhang; (b) 0.6 m overhang, (c) 0.9 m overhang and (d) 1.2 m overhang

With overhangs added (Fig. 6b-6d), the majority of the catch ratios (i.e. at locations without overhang) on the east facade are similar to that of the monitoring period without overhang since both prevailing wind directions are from the east with similar wind speeds and horizontal rainfall intensities. However, it is evident that the gauges below the overhang have much lower catch ratios when compared to: (1) other gauges of similar height and distance from edge and (2) the same gauges during the monitoring period without overhang. The gauges right below the overhang are the most protected (EN1, EN5, EN8).

Figure 7 shows the catch ratios calculated over the four periods on the north façade. Since the prevailing wind direction is from the east, the catch ratios on the north facade are not symmetrical and are much

lower than that on the east façade. The gauges on the left edge of the facade (NE1 and NE2) receive less rain than the gauges located to their right. This may be explained by considering the wind flow around the building. Since the prevailing wind direction during rain hours is from the east, flow separation occurs at the edges of the east facade, resulting in a wetting pattern that is reflective of the wind flow around the north-east edge. The locations right below the overhang (NE3 and NC1) are the most protected having significantly lower catch ratios when compared to NW1 (Fig. 7b-d), which is at the same height. This is also apparent when compared to the north facade without overhang (Figure 7a). The remaining locations below the overhang are protected to various degrees.

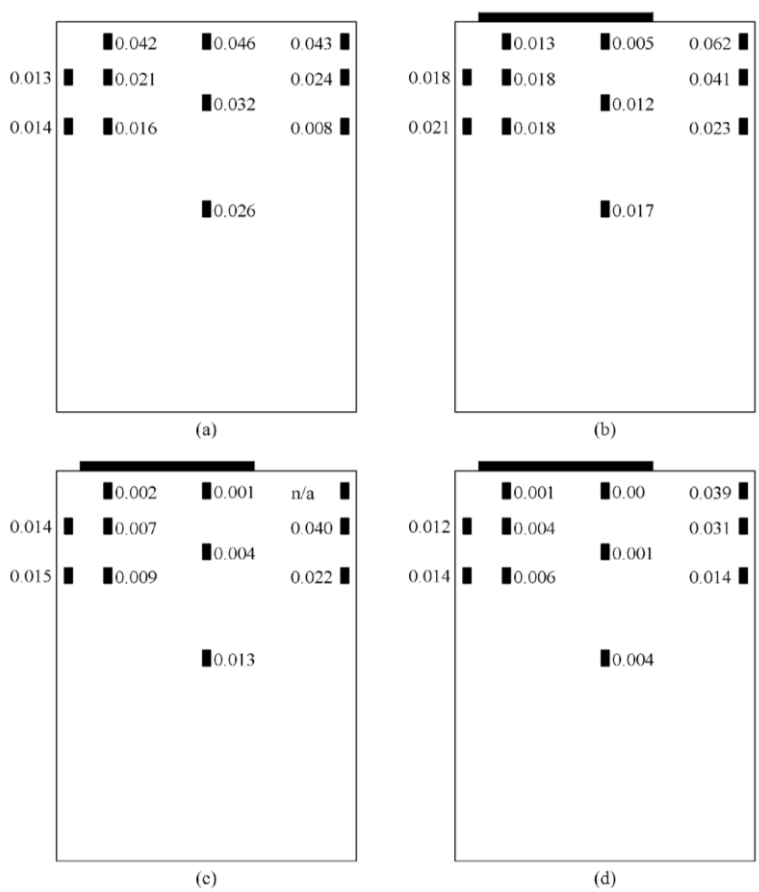

Figure 7: Catch ratio on the north facade: (a) no overhang; (b) 0.6 m overhang; (c) 0.9 m overhang and (d) 1.2 m overhang

Effectiveness of Overhang

The effectiveness of overhang, δ, is defined as the percentage reduction in catch ratios with and without the overhang. The overhang effectiveness is assessed by two approaches: 1) similarity, which compares two similar rain events during the periods with and without overhang; and 2) symmetry, which uses a symmetrical distribution of WDR across the building facade during a rain event.

$$\delta = \frac{\eta - \eta_{OH}}{} \times 100 \qquad (2)$$

Where η is the catch ratio without overhang, η_{OH} is the catch ratio with overhang.

Similarity

The overhang effectiveness can be assessed by comparing the catch ratios at the gauge locations that are directly under the overhang (gauges EN1 to EN9) in one rain event with the catch ratios at the same gauge locations in a similar rain event without overhang. To establish similarity, both rain events should have similar meteorological characteristics, i.e. wind speed, wind direction and rainfall intensity, ultimately leading to similar catch ratios at the gauge locations that are not influenced by the overhang. Once this similarity has been established, the catch ratios at gauge locations EN1 to EN9 (under the overhang) during rain events without overhang can be compared to the catch ratios during rain events with overhang.

As an example, Table 1 shows the catch ratios on the east façade for two similar rain events, RE 6 during the period without overhang, and RE 54 during the period with the 0.9 m overhang. The comparison of onsite meteorological data indicates similar wind and rain characteristics between these two rain events that yield similar catch ratios on the gauges not sheltered by the overhang, which are the un-shaded values (EC1, EC2, ES1 to ES7). The wind and rain characteristics of these two rain events: (1) RE6: Oct. 12 2013 to Jan. 02 2014; total rainfall amount=111.5mm, no. of rain hours=161 hours, average wind speed =1.52m/s, average arithmetic wind direction=120o and average rain fall intensity=0.7mm/hr. (2) RE54: Oct. 19 2016 to Oct. 30 2016; Total rainfall amount=103.4mm, no. of rain hours=110 hours, average wind speed =1.64m/s, average arithmetic wind direction=115o, average rain fall intensity=1mm/hr.

Table 1: Catch ratios and overhang effectiveness on the east façade for rain events 6 and 54.

WDR Gauge	Catch Ratios		Overhang Effectiveness (%)
	RE 6 (No OH)	RE 54 (0.9 m OH)	
EN1	0.108	0.022	80
EN2	0.096	0.036	63
EN3	0.049	0.042	15
EN4	0.038	0.026	33
EN5	0.093	0.003	97
EN6	0.050	0.012	76
EN7	0.034	0.012	63
EN8	0.093	0.001	99
EN9	0.045	0.010	78
EC1	0.101	0.105	
EC2	0.021	0.018	
ES1	0.111	0.101	
ES2	0.062	0.061	
ES3	n/a	0.054	
ES4	0.025	0.019	
ES5	0.085	0.100	
ES6	0.057	0.044	

ES7	**0.035**	**0.029**

**** Shaded rows catch ratios for WDR gauges located under the retractable overhang. Data for gauge ES3 was not available during this period due to hardware malfunction.***

A number of similar rain events are identified for each overhang size. The percentage reduction in catch ratios, i.e. overhang effectiveness, is calculated for each pair of rain events. Given that the WDR deposition on façade is highly dependent on the meteorological parameters and that the catch ratios vary over different rain events, each comparison yields a different percent reduction in catch ratio for the same gauge location and an average is used to report the effectiveness of overhangs.

Symmetry

As shown in Figure 6, the catch ratios are more or less symmetrical on the east façade given that the predominant wind direction is from the east during rain hours, which is normal to the façade. Therefore, a symmetrical distribution of WDR can be assumed to evaluate the effectiveness of overhang by directly comparing the catch ratios at gauge locations underneath the overhang on the north side of the façade (EN1 to EN7) to those on the south side of the façade (ES1 to ES7), which do not have an overhang above them. Rain events with the prevailing wind direction coming from the east are selected and the percentage reduction in catch ratios for all three overhang sizes are calculated. The meteorological parameters between rain events differ from one another resulting in different percent reductions in catch ratio for the same gauge location, therefore, the average is used to report the effectiveness of overhangs.

Similarity versus Symmetry

The average percentage reductions in catch ratio calculated for gauge locations on the east façade using both methods are compared (Figure 8). In general, there is a good agreement between these two methods with a difference between 0 to 21%. For the 0.6 m overhang, the average percent reductions calculated using the similarity approach are slightly higher than those calculated using the symmetry approach. The highest discrepancy is for gauge EN2 (14%) and less than 10% for other gauges. For the 0.9 m overhang the highest difference is for gauges EN3 and EN 7 with 16% and 11% difference, respectively and less than 5% for other gauges. Regarding the 1.2 m overhang, the average percent reductions in catch ratios are almost identical for both methods (0-7% difference) with the exception of EN4 with the difference of 21%.

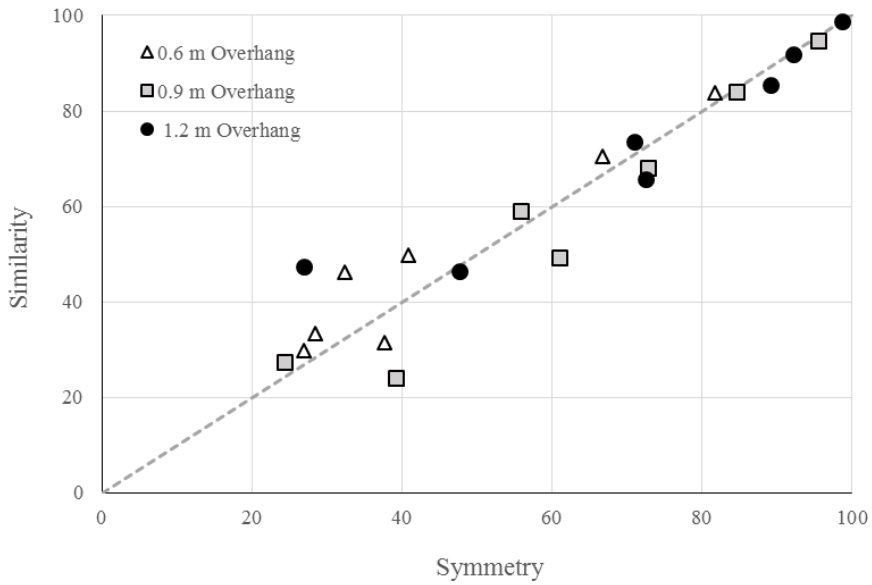

Figure 8: Comparison of overhang effectiveness calculated using similarity and symmetry approaches for gauges on the east façade

Quantification of Overhang Efficiency

Given the similar results obtained by similarity and symmetry approaches and the fact that predominantly easterly winds do not allow for symmetry analysis on the north facade, similarity method is used to calculate the effectiveness of overhang for the north façade. However, for the east façade, the average calculated using these two methods is used for the analysis presented in this section.

Figure 9 and Figure 10 show the effectiveness of overhang on the east façade and north façade, respectively. Similar trend is observed on both façades. In general, with the increase of overhang size, the protection, i.e. overhand effectiveness, increases. The effectiveness of the overhang decreases when moving from the upper edge towards the ground and from the center towards the side edge of the façade. The overhang reduces the WDR deposited on the façade, especially the area immediately beneath the overhang (EN1, EN5, EN8, NE3, NC1 at 0.6 m below the roofline, i.e. 3% of the building height).

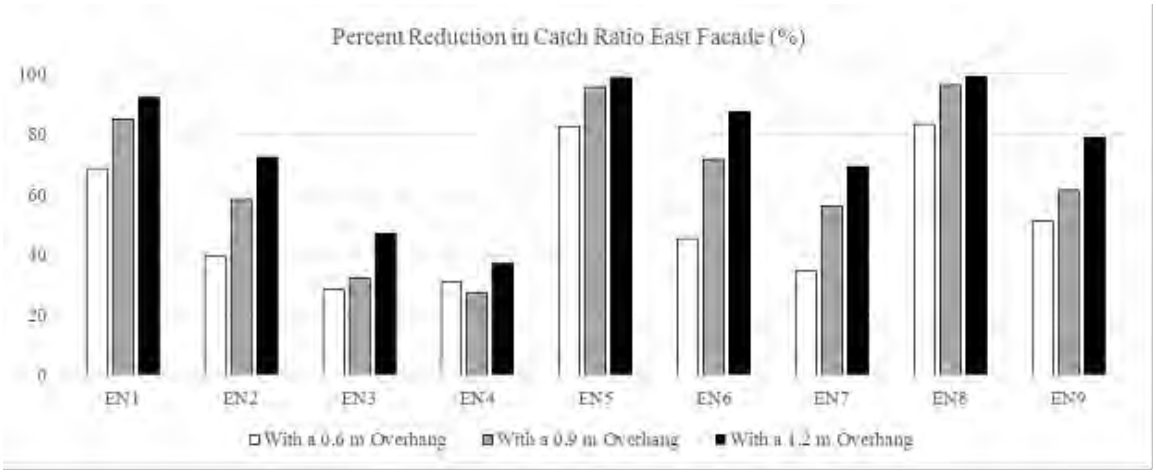

Figure 9: Effectiveness of overhangs on the east façade

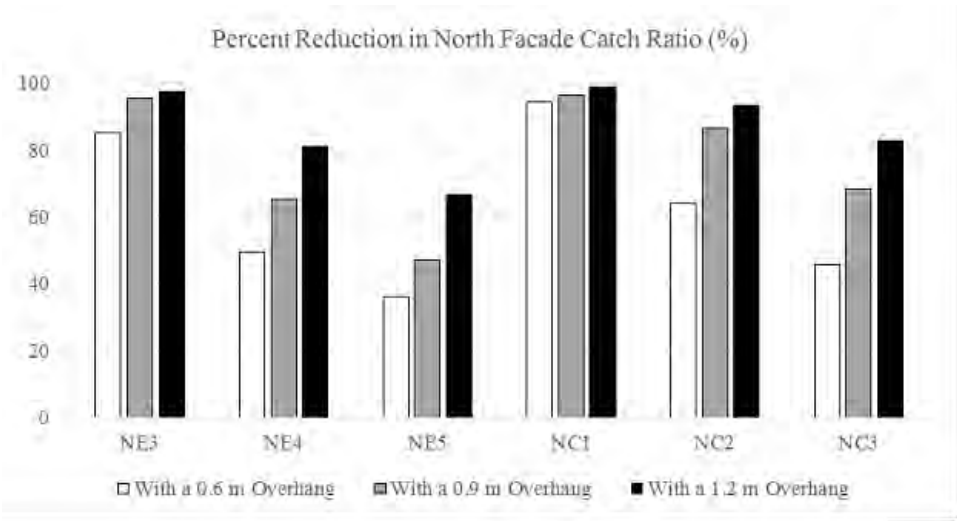

Figure 10: Effectiveness of overhangs on the north façade

The overhang effectiveness is also plotted in relation to the normalized building height, as shown in Figure 11 for the east façade. With the increase of distance from the roofline, the overhang effectiveness decreases, which exhibits a quasi-linear relationship. At a distance of 0.6 m below the roofline (i.e. 3% of the building height), the overhang effectiveness ranges from 70% to 99% for the three different overhang sizes, while the overhang effectiveness is reduced to a range of 30-80% at a distance of 4.9 m below the roofline (i.e. ¼ of the building height, EN3, EN7, EN9). The protection area can extend up to 9.1 m below the roofline (i.e. about 45% of the building height, EN4) with a similar amount of WDR reduction of about 30% as at a distance of 4.9 m below the roofline for 0.6 m and 0.9 m overhang, while the overhang effectiveness is slightly higher, i.e. 37%, at this location for 1.2 m overhang. A similar trend is observed for the north façade.

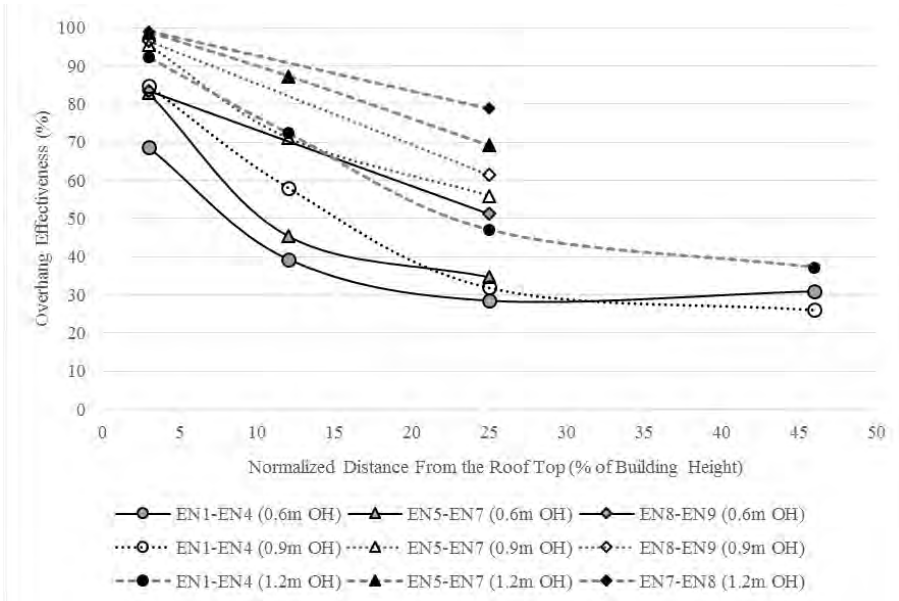

Figure 11: Effectiveness of overhangs on the east façade with regard to distance from the roofline

To quantify the effect of overhang on the reduction of WDR impinged on the façade, an area-weighted average catch ratio ($\bar{\eta}$) is introduced (equation 3) to calculate the area-weighted overhang effectiveness for four areas shown in Figure 12, namely A1, A2, A3 and A4 representing 15%, 30%, 60% and 100% of the façade area, respectively. This evaluation is carried out for the case that the entire façade width is fitted with overhang (i.e. full overhang) for both east and north facades.

$$\bar{\eta} = \frac{1}{\sum_{i=1}^{n} A_i} \sum_{i=1}^{n} \eta_i A_i \tag{3}$$

where, the summation index i is the cell number, A_i is the area of the ith cell and n is the total number of the cells over which the average is calculated. The façade is divided into cells in such a way that rain gauges are located in the centre of a cell. There are twenty-five cells, five columns and five rows on the east façade. For the cells with rain gauge, a constant catch ratio is assigned with value measured by the gauge located in its centre. For the remaining nine cells located at the lower and centre parts of the façade, a constant catch ratio interpolated from the adjacent cells is assigned. For these areas, the catch ratios are quite small.

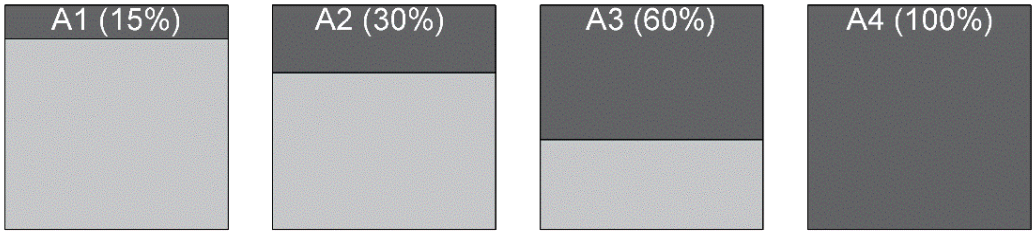

Figure 12: Areas on the east façade for the calculation of area-weighted overhang effectiveness.

Table 2: Effect of full overhang on WDR reduction on the east façade

Façade area	No overhang		0.6 m overhang		0.9 m overhang		1.2 m overhang	
	$\sum_{i=1}^{n} \eta_i A_i$	WDR distribution on façade (%)	$\sum_{i=1}^{n} \eta_i A_i$	Area-weighted effectiveness (%)	$\sum_{i=1}^{n} \eta_i A_i$	Area-weighted effectiveness (%)	$\sum_{i=1}^{n} \eta_i A_i$	Area-weighted effectiveness (%)
A1 (15%)	18.2	53.0	6.41	65	4.09	77	2.10	92.2
A2 (30%)	23.2	67.6	9.84	58	6.68	71	3.84	86.8
A3 (60%)	29.9	87.4	14.38	52	11.57	61	8.11	77.7
A4 (100%)	34.3	100	18.70	45	15.89	54	12.43	68.0
Total WDR reduction (%)			45		54		68	

As shown in Table 2, without overhang, the top 15% of the façade area receives 53% of the total WDR and the top 30% of the façade area receives about 70% of the total WDR impinged on the entire façade. With a 0.6 m overhang added, the 53% of WDR impinged on the top 15% of façade area can be reduced by 65%, which is 35% reduction of the total amount and this reduction can be increased to about 50% when a 1.2m overhang is added. These results show that the addition of an overhang is effective in significantly reducing WDR amount especially for the top area. The total amount of WDR impinged on the façade can be reduced by 45% with a 0.6 m overhang, 54% with a 0.9 m overhang and by 68% with a 1.2 m overhang, respectively. A linear relationship exists between the overhang width and the amount of WDR deposited on façade, as shown in Figure 13. The results obtained for north façade are very similar to those observed on the east façade.

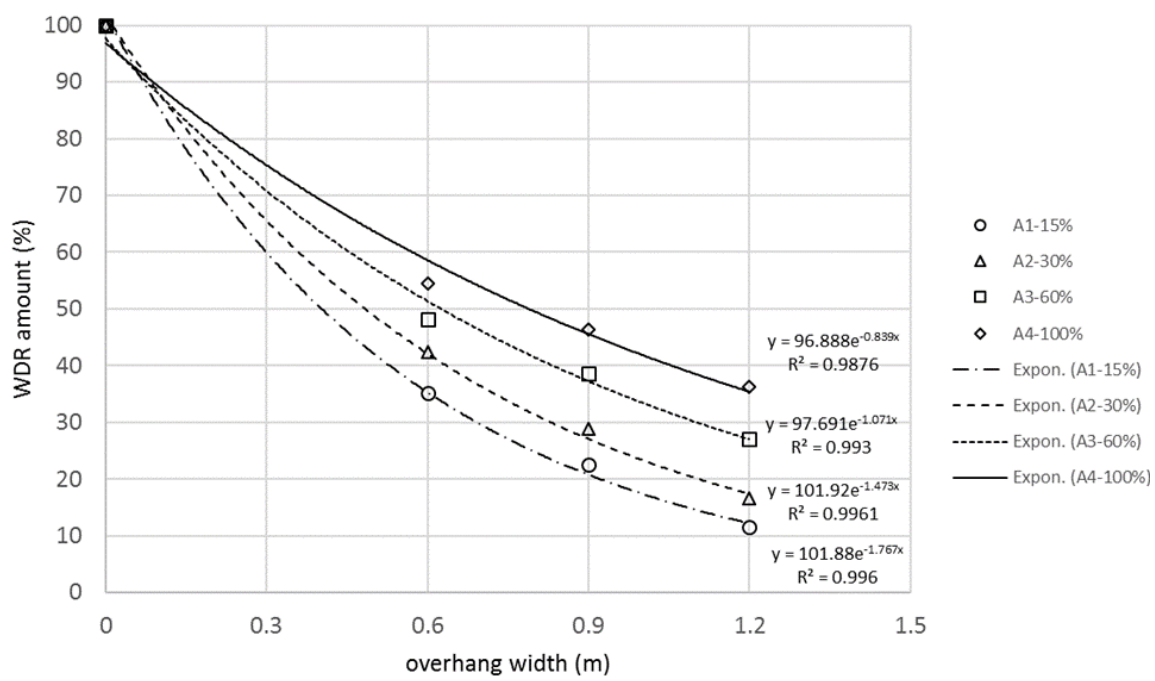

Figure 13: Relationship between overhang width and the amount of WDR deposited on east façade for four different areas.

CONCLUSIONS

The effectiveness of overhang on reducing WDR on façade has been studied through field measurements by fitting a retractable overhang on a six-story building located in Vancouver. On-site weather data and WDR on façade have been collected for four overhang widths over a period of four years. The main findings are:

- For the particular climate characterized by long rainy winters with mild wind and rain, the overhang is effective and significantly reduces WDR for this six-story building, especially for areas directly underneath the overhang.
- The protection increases from the side edge to the center and from the bottom to the top of the façade.
- The protection provided by the overhang can extend to about half building height.
- Given that about 70% of the total amount of WDR impinged on the façade is received by the top 30% of the façade area, overhangs that can shelter the top 30% of the façade can effectively protect the façade from WDR wetting. A 0.6 m overhang can reduce the total amount of WDR by 45% on this six-story building.
- As expected, the larger overhang provides a greater protection. An exponential relationship with good correlation of overhang width and its effectiveness has been observed based on the data points available.

ACKNOWLEDGEMENTS

The authors are grateful for the financial support received from NSERC Strategic Research Network for Engineered Wood-based Building Systems (NEWBuildS), Homeowner Protection Office branch of BC housing, and the Faculty of Engineering and Computer Science of Concordia University.

The authors would like to acknowledge the great efforts made by Dr. Paul Morris in initiating and supporting this research project through NEWBuildS. It was with his impetus and persistence that this project was made possible. The authors would also like to thank Dr. Jieying Wang and Daniel Wong from FP Innovations for their assistance in the data collection.

REFERENCES

Abuku M, Blocken B, Nore K, Thue JV, Carmeliet J, Roels S., 2009. On the validity of numerical wind-driven rain simulation on a rectangular low-rise building under various oblique winds. Building and Environment; 44(3): 621-632.

Blocken B. and Carmeliet, J. 2002. Spatial and temporal distribution of driving rain on a low-rise building. Wind and Structures 5(5):441-462.

Blocken, B. and Carmeliet, J., 2004. A review of wind-driven rain research in building science. Journal of Wind Engineering and Industrial Aerodynamics; 92 (13): 1079-1130.

Blocken B. and Carmeliet, J. 2005. High-resolution wind-driven rain measurements on a low-rise building—experimental data for model development and model validation. Journal of Wind Engineering and Industrial Aerodynamics; 93(12): 905–928.

Blocken, B. and Carmeliet, J., 2006. Validation of CFD simulations of wind-driven rain on a low-rise building façade. Building and Environment; 42(7):2530-2548.

Blocken B. and Carmeliet J. 2006. The influence of the wind-blocking effect by a building on its wind-driven rain exposure. J. of Wind Engineering and Industrial Aerodynamics; 94: 101-127.

Blocken, B., Dezsö, G., Beeck, J. V., and Carmeliet, J., 2009. The mutual influence of two buildings on their wind-driven rain exposure and comments on the obstruction factor. Journal of Wind Engineering and Industrial Aerodynamics; 31: 1-21.

Blocken, B. and Carmeliet, J., 2010. Overview of three state-of-the-art wind-driven rain assessment models and comparison based on model theory. Building and Environment. 45(3): 691-703.

Blocken, B., Abuku, M., Nore, K., Briggen, P. M., Schellen, H. L., Thue, J. V., Roels, S., and Carmeliet, J., 2011. Inter-comparison of wind-driven rain deposition models based on two case studies with full-scale measurements. Journal of Wind Engineering and Industrial Aerodynamics; 99(4): 448-459.

Briggen, P.M., B. Blocken and H.I. Schellen. 2009. Wind-driven rain on the façade of a monumental tower: numerical simulation, full-scale validation and sensitivity analysis. Building and Environment; 44 (8): 1675-1690.

Chiu, V. 2016. The effect of overhang on wind-driven rain wetting of a mid-rise building. M.A.Sc thesis. Concordia University, Montreal, Canada.

CMHC, 1996. Survey of building envelope failures in the coastal climate of British Columbia. Canadian Mortgage and Housing Corportion, Ottawa.

Deb Nath, K. U., V., Chiu, and H. Ge. Measurements of wind-driven rain on mid- and high-rise buildings in three Canadian regions. Proceedings of the 6th International Building Physics Conference: Building Physics for a Sustainable Built Environment. Turin, Italy. June 14-17, 2015.

Derome, D., A. Kubilay, T. Defraeve, B. Blocken and J. Carmeliet. 2017. Ten questions concerning modeling of wind-driven rain in the built environment. Building and Environment; 114:495-506.

Etyemezian, V., C.I. Davidson, M. Zufall, W. Dai, S. Finger, M. Striegel. 2000. Impingement of rani drops on a tall building. Atmospheric Environment; 34:2399-2412.

Foroushani, S., Ge, H. and Naylor, D. 2013. Effects of roof overhangs on wind-driven rain wetting of a low-rise cubic building: a numerical study. Journal of Wind Engineering and Industrial Aerodynamics; 125: 38-51.

Ge, H. and Krpan, R. 2009. Wind-driven rain study in the Coastal Climate of British Columbia. Research report submitted to Canadian Mortgage and Housing Corporation, Ottawa. https://www.bchousing.org/publications/WindDrivenRainStudy.pdf

Huang, S. H., and Li, Q.S. 2010. Numerical simulations of wind-driven rain on building envelopes based on Eulerian multiphase model. Journal of Wind Engineering and Industrial Aerodynamics; 98(12): 843-857.

Inculet, D. and Surry, D. 1995. Simulation of wind-driven rain and wetting patterns on buildings. Research report for Canadian Mortgage and Housing Corporation, Ottawa.

Kubilay, A., Derome, D, and Blocken, B. 2013. CFD simulation and validation of wind-driven rain on a building facade with an Eulerian multiphase model. Building and Environment; 61: 69-81.

Kubilay, A., D. Derome, B. Blocken, and J. Carmeliet. 2014. Numerical simulations of wind-driven rain on an array of low-rise cubic buildings and validation by field measurements. Building and Environment. 81:283-295.

Kubilay A, Derome D, Blocken B, and Carmeliet J., 2014. High-resolution field measurements of wind-driven rain on an array of low-rise cubic buildings. Building and Environment. 78: 1-13.

Kubilay, K., D. Derome, B. Blocken, and J. Carmeliet. 2015. Wind-driven rain on two parallel wide buildings: field measurements and CFD simulations, Journal of Wind Engineering and Industrial Aerodynamics; 146:11-28.

Kubilay, A., D. Derome, B. Blocken, and J. Carmeliet. 2015. Numerical modeling of turbulent dispersion for wind-driven rain on building facades, Environmental Fluid Mechanics; 15 (1):109-133.

Kubilay, A., D. Derome, and J. Carmeliet, 2017. Analysis of time-resolved wind-driven rain on an array of low-rise cubic buildings using large eddy simulation and an Eulerian multiphase model. Building and Environment. 114: 68-81.

Kubilay, A., Carmeliet J. and Derome, D. 2017. Computational fluid dynamics simulations of wind-driven rain on a mid-rise residential building with various types of façade details. Journal of Building Performance Simulation; 10 (2): 125-143.

Kumaran, K. and Sanders, C., 2008. IEA Annex 41, Final report, Volume 3. Whole Building Heat, Air, Moisture Response - Boundary Conditions and Whole Building HAM Analysis. International Energy Agency.

Lakehal, D., Mestayer, P.G., Edson, J.B., Anquetin, S., and Sini, J.E. 1995. Eulero-Lagarangian simulation of raindrop trajectories and impacts within the urban canopy. Atmospheric Environment; 29(23):3501-3517.

Morris, P.I., 2006, Damp costal weather field issues and improving performance. Wood Protection, H.M. Barnes, Ed. Forest Products Soc., Madison, Wisconsin. pp. 165-171.

Nore, K., Blocken, B., Petter Jelle, B., Thue, J.V., and Carmeliet, J., 2007. A dataset of wind-driven rain measurements on a low-rise test building in Norway. Building and Environment. 42(5):2150-2165.

Pettersson, K., S. Krajnovic, A.S. Kalagasidis and P. Johansson. 2016. Simulating wind-driven rain on building facades using Eulerian multiphase with rain phase turbulence model. Building and Environment 106: 1-9.

Zhu, D., Mallidi, S.R., Fazio, P., 1995, Quantitative driven rain exposure on a vertical wall at various Canadian cities. Building and Environment 30 (4): 533-544